




Facile construction of single-crystalline sodium niobate anode materials: insight into the relationship of the morphology and excellent performance for lithium-ion batteries

Zhengyu Du¹, Qianqian Liu^{1,*} , Miao Cheng¹, Jing Hu¹, Tao Wei¹, Wanfei Li^{1,*}, Yun Ling¹, Xufei Hu¹, and Bo Liu^{1,*}

¹Suzhou Key Laboratory for Nanophotonic and Nanoelectronic Materials and Its Devices, School of Materials Science and Engineering, Suzhou University of Science and Technology, Suzhou 215009, Jiangsu Province, China

Received: 5 November 2021

Accepted: 22 February 2022

Published online:

7 March 2022

© The Author(s), under exclusive licence to Springer Science+Business Media, LLC, part of Springer Nature 2022

ABSTRACT

Electrode materials structures hold the key to enhance the performance. Based on the time-dependent growth process of niobium precursor, single-crystal $\text{Na}_2\text{Nb}_2\text{O}_6 \cdot n\text{H}_2\text{O}$ nanowires and NaNbO_3 nanocubes were successfully synthesized through a facile and friendly hydrothermal route at 180 °C under different reaction times. NaNbO_3 nanowires were derived by calcination treatment of $\text{Na}_2\text{Nb}_2\text{O}_6 \cdot n\text{H}_2\text{O}$ nanowires which was employed as self-sacrificing templates. By comparing the electrochemical behavior of these niobium-based anodes, NaNbO_3 nanocubes show a discharge capacity of about 115 mA h g⁻¹ over 1000 cycles at 1000 mA g⁻¹, exhibiting higher reversible capacity and superior rate performance than NaNbO_3 nanowires. The superior cell performance could be interpreted in terms of the different morphologies of NaNbO_3 , which results in the better Li-ion diffusion abilities and higher pseudo-capacitance of the as-fabricated NaNbO_3 nanocubes electrode. This work provides fundamental insights into the morphology–property relationship of both NaNbO_3 nanowires and NaNbO_3 nanocubes, providing a solid guide for developing anode materials for Li-ion battery.

Handling Editor: Mark Bissett.

Zhengyu Du and Qianqian Liu have equally contributed to this work.

Address correspondence to E-mail: liuqianqian@usts.edu.cn; wfli2018@mail.usts.edu.cn; liubo@mail.usts.edu.cn

<https://doi.org/10.1007/s10853-022-07048-4>

Introduction

Nowadays, lithium-ion batteries (LIBs) are the most widely used energy storage devices for powering portable devices and electrical vehicles [1–3]. However, due to their high-rate poor security and deteriorated cycling performance limited by the rate performance of commercial graphite anodes, traditional lithium-ion batteries cannot achieve the rapidly increasing high power energy storage requirements [4, 5]. Exploring safe and high-performance anode materials for LIB has been the focus of much research. Niobium-based materials are demonstrated to be promising anode candidates for high-rate energy storage applications, because they have fast kinetics of the electrochemical ion insertion and extraction. To date, a number of niobium-based materials, especially niobium-based oxides with multiple redox couples ($\text{Nb}^{5+}/\text{Nb}^{4+}$ and $\text{Nb}^{4+}/\text{Nb}^{3+}$), have attracted much attention because of their high specific capacities. As the most studied molecule of the niobium-based oxides, Nb_2O_5 featured with high working voltage and a large practical capacity have drawn ever-increasing attention as anode materials for LIBs. But its poor electronic conductivity and capacity retention that resulting in insufficient rate capability and shortened cycling life greatly restrict its applicability [6–10]. To obtain more outstanding niobium-based oxide anodes, various strategies, such as introducing other metal elements into Nb_2O_5 , have been adopted [11, 12]. As a result, intercalation-type M-Nb-O anode materials have been studied worldwide due to their safe operating potentials, high specific capacities, high cycling stability, and significant intercalation pseudocapacitive behavior.

M-Nb-O compounds based on transition metals and alkaline earth metal including Ti-Nb-O [13–15], Fe-Nb-O [16–18], Ga-Nb-O [19, 20], Cr-Nb-O [21], Zr-Nb-O [22, 23], W-Nb-O [24, 25], Mg-Nb-O [26], Ba-Nb-O [27] are reported to be fabricated and used as anode materials for LIBs. However, the synthetic route of the above M-Nb-O materials always involves complicated processes and high calcination temperatures. NaNbO_3 , as a new member of M-Nb-O materials based on alkali metal, has attracted particular research attention in recent years due to its simple green synthesis route and excellent photo-physical and chemical properties. While NaNbO_3 has

been widely used as piezoelectric materials, ferroelectric materials, biological detection reagents and photocatalytic materials, the application of NaNbO_3 for LIBs has not been explored until Yan et al. reported NaNbO_3 micro-/nano-crystals as anode for Li-ion storage, and then revealing its pseudocapacitive intercalation mechanism [28]. It is well known that the performance of an electrochemical performance of an electrode material greatly depends on its morphology and microstructure because different structures can afford different effective surface areas and electroactive sites as well as conductive networks [29–36]. However, to date, comparative investigating the effect of morphologies of NaNbO_3 on the performance for LIBs is still lacking.

Herein, the electrochemical performances of controllable NaNbO_3 nanowires and NaNbO_3 nanocubes were explored for LIB. NaNbO_3 with tunable morphology was prepared combined a facile and friendly hydrothermal route. The NaNbO_3 nanowires were obtained after hydrothermal time of 2 h and a heat-treat at 500 °C for 12 h, while NaNbO_3 nanocubes were easy prepared by the hydrothermal treatment time of 3 h. Their electrochemical performances as anodes for LIBs were investigated. Meanwhile, the effects of NaNbO_3 morphology on Li-ion diffusion abilities and storage were intensively studied. Morphological control can result in the increase of Li-ion diffusion kinetics and Li storage of NaNbO_3 nanocubes, which deliver a higher discharge capacity of about 115 mA h g^{-1} over 1000 cycles at 1000 mA g^{-1} and exhibit higher rate capability than those of NaNbO_3 nanowires prepared in this work.

Materials and methods

Materials synthesis

All materials were analytical reagents, which were used without any purification. Nb_2O_5 (purity, 99.5%) and sodium hydroxide (purity, 99%) were obtained from Sinopharm Chemical Reagent Co., Ltd. NaNbO_3 nanowires were synthesized through the combination of a hydrothermal method and calcination following a time-dependent growth process. In a typical synthetic process, Nb_2O_5 (1.00 g, 3.76 mmol) was added into a solution of NaOH (10 M, 60 mL) and then transferred into Teflon-lined stainless-steel autoclave. The autoclave was held at 180 °C for 2 h. After the

reaction, the autoclave was naturally cooled to room temperature. The obtained white solids were washed with ethanol and deionized water several times to remove the impurities. Then, the as-prepared products were placed in a vacuum drying oven at 100 °C for 24 h, and niobium precursors of $\text{Na}_2\text{Nb}_2\text{O}_6 \cdot n\text{H}_2\text{O}$ nanowires were obtained. Subsequently, $\text{Na}_2\text{Nb}_2\text{O}_6 \cdot n\text{H}_2\text{O}$ nanowires were calcined at 500 °C for 12 h in a muffle and converted into NaNbO_3 nanowires. NaNbO_3 nanocubes were synthesized through the same hydrothermal procedure with a reaction time increasing to 3 h.

Material characterizations

XRD characterization was performed on a Bruker D8 Focus X-ray diffractometer using $\text{Cu K}\alpha$ radiation ($\lambda = 1.5406 \text{ \AA}$) in the 2θ range from 10 to 60°. SEM characterization was performed on a Hitachi SU-70 SEM instrument. TEM characterization was performed on a JEOL JEM-2100 TEM instrument.

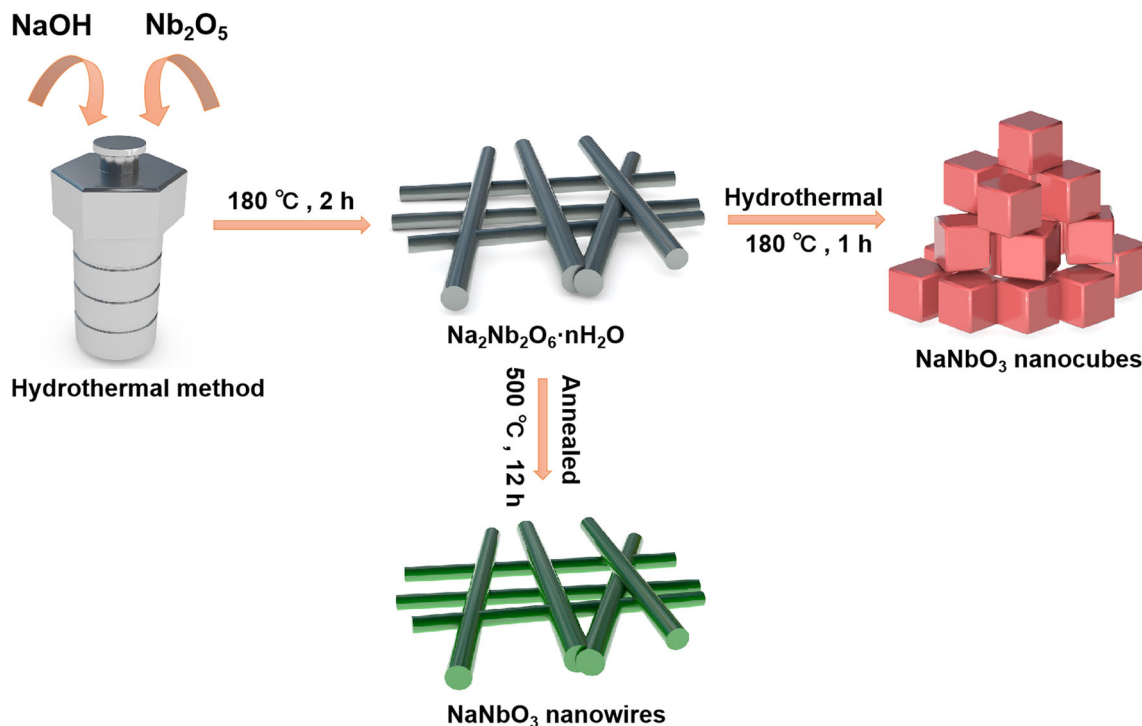
Electrochemical measurements

The electrochemical performance was evaluated by using CR2016-type coin cells that were assembled in a glove box filled with highly pure Ar gas (< 1 ppm of oxygen and water). The working electrodes were prepared by using N-methylpyrrolidone (NMP)-based slurry containing active materials (NaNbO_3 nanowires or nanocubes), conductive carbon black (Super P), and binder (PVDF) in a mass ratio of 65:25:10. The loading mass of active materials in the final working electrode is around $1 \sim 1.5 \text{ mg cm}^{-2}$. Metallic Li plates were used as counter electrodes. The electrolyte was made up of 1 M LiPF_6 in the mixture of ethylene carbonate (EC), diethylene carbonate (DEC) and dimethyl carbonate (DMC) (EC/DEC/DMC = 1:1:1, volume ratio). Galvanostatic charge/discharge performances were carried out using a CT2001 automatic battery tester (LAND, China). Cyclic voltammetry (CV) and electrochemical impedance spectroscopy (EIS) tests were performed on a VMP-3 electrochemical workstation (Bio-Logic, France).

Results and discussion

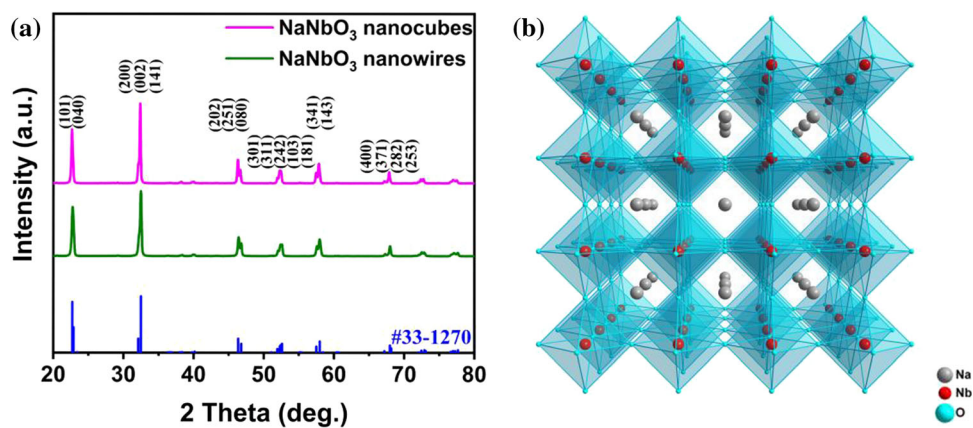
A typical schematic illustration for the synthesis of NaNbO_3 nanowires and NaNbO_3 nanocubes is illustrated in Scheme 1. The niobium and sodium sources were provided by niobium pentoxide and sodium hydroxide, respectively. Using a hydrothermal reaction, we first fabricated white solid precursor of $\text{Na}_2\text{Nb}_2\text{O}_6 \cdot n\text{H}_2\text{O}$ nanowires from niobium pentoxide and sodium hydroxide at 180 °C for 2 h. Subsequently, niobium precursor of $\text{Na}_2\text{Nb}_2\text{O}_6 \cdot n\text{H}_2\text{O}$ nanowires was calcined at 500 °C for 12 h affording NaNbO_3 nanowires, which essentially retained the corresponding morphologies of niobium precursor. Considering the higher thermodynamic stability of NaNbO_3 nanocubes and the characteristics of $\text{Na}_2\text{Nb}_2\text{O}_6 \cdot n\text{H}_2\text{O}$ nanowires' metastable phase, it is anticipated that the longer hydrothermal reaction time will promote the transformation of $\text{Na}_2\text{Nb}_2\text{O}_6 \cdot n\text{H}_2\text{O}$ nanowires to NaNbO_3 nanocubes. Upon prolong the hydrothermal reaction time to 3 h, the precursor of $\text{Na}_2\text{Nb}_2\text{O}_6 \cdot n\text{H}_2\text{O}$ nanowires was converted gradually into single-crystal NaNbO_3 nanocubes. It is noted that this synthetic route is able to provide a low-cost, facile and potential scale-up technology for obtaining high-quality NaNbO_3 nanocubes and nanowires in high yield, easily in the gram scale for one batch experiment.

The X-ray diffraction (XRD) patterns of the as-prepared NaNbO_3 nanocubes and nanowires are presented in Fig. 1a, in which the sharp diffraction peaks imply the good crystalline of the products. Similarly, to previously reported ones, the single-crystal NaNbO_3 obtained in this work exhibits the characteristic XRD peaks, which are in good agreement with the values given in the standard card of the orthorhombic phase (JCPDS 33–1270). The positions of the main diffraction peaks for NaNbO_3 appear at around 22.7, 22.9, 32.1, and 32.5°, which correspond to the (101), (040), (200), (002), (141) crystal faces, respectively. No peaks of impurity are observed in the XRD pattern, indicating the high purity of obtained NaNbO_3 samples. The crystal structure of orthorhombic NaNbO_3 is shown in Fig. 1b and is similar to a typical perovskite structure, in which NbO_6 octahedron as an elementary component and all NbO_6 octahedrons are connected at the corners forming the 3D framework with Na^+ ions incorporated in between the sheets. Such stable interconnected microchannel structure is significantly



Scheme 1 Schematic diagram for the fabrication of NaNbO₃ nanocubes and nanowires.

Figure 1 **a** XRD patterns of NaNbO₃ nanocubes and NaNbO₃ nanowires, **b** crystal structure of NaNbO₃.



in favor of the rapid Li⁺ ion transportation and high cycling stability. The lattice parameters and unit-cell volumes calculated from the XRD data show that for NaNbO₃ nanocubes, these values become larger compared to that of NaNbO₃ nanowires (Table S1). It is well known that the increased unit volume can expand the transmission path of Li⁺ in its lattice [37], which is beneficial to significantly improve the ionic conductivity and electrochemistry of NaNbO₃ nanocubes as anode material for Li-ion battery [38, 39].

The morphology and structure of NaNbO₃ products were examined by scanning electron microscope (SEM) and transmission electron microscope (TEM).

Figure 2a and e depicts the SEM images of the NaNbO₃ nanowires and nanocubes, respectively. It could be seen that 1D wire-like crystals with average dimensions of 200 nm in diameter and tens of micrometers in length were successfully synthesized by the feasible hydrothermal synthesis, which consistent with the results of the TEM images (Fig. 2a and b). While NaNbO₃ nanocubes were prepared with size ranges from 0.5 to 1.5 μm (Fig. 2e and f). The high-resolution TEM (HRTEM) images demonstrated the NaNbO₃ nanowires and nanocubes were well crystallized, as evidenced by the clear and orderly lattice fringes (Fig. 2c and g). Meanwhile, the

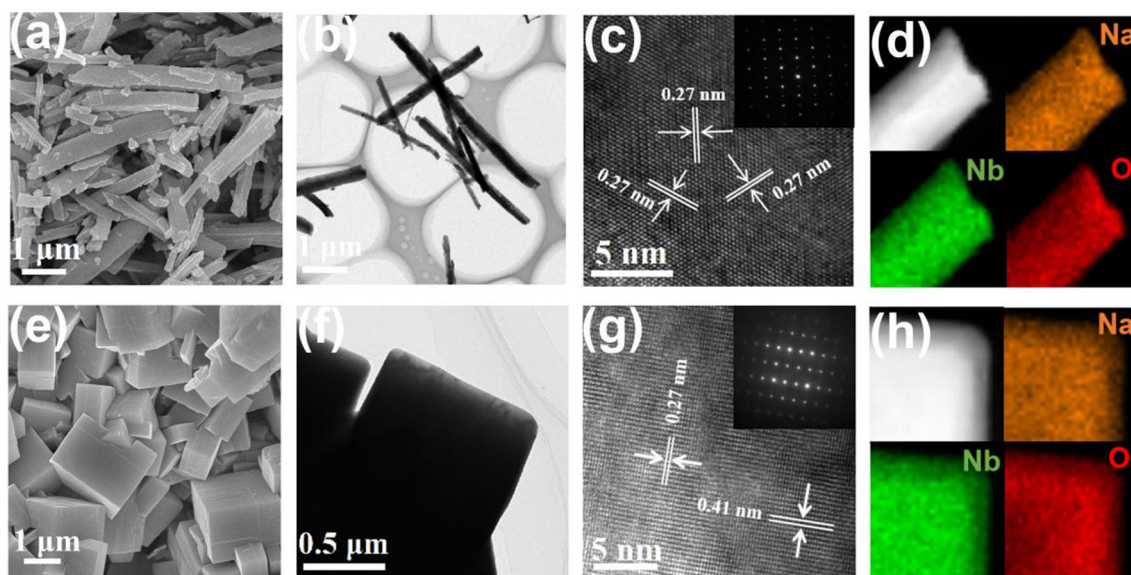


Figure 2 a, b, c SEM, HRTEM and SAED images of NaNbO_3 nanowires. e, f, g SEM, HRTEM and SAED images of NaNbO_3 nanocubes. d, h TEM and corresponding EDS elemental mapping

images of Na, Nb, O elements in NaNbO_3 nanowires and NaNbO_3 nanocubes.

lattice spacing in the HRTEM images is 0.27 nm and 0.41 nm (Fig. 2c and g), matching to the (200) and (101) crystallographic planes of NaNbO_3 . Additionally, the SAED patterns perfectly match with the orthorhombic structure ($P2/m$ space group), indicating its single-crystalline character. These HRTEM and SAED results are in good agreement with the XRD analyses. The X-ray energy-dispersive spectra (EDS) elemental mapping images (Fig. 2d and h) show the presence of O, Na and Nb elements and uniform distribution of these elements in the NaNbO_3 products.

The electrochemical performances of as-obtained NaNbO_3 nanocubes and nanowires as anode for LIB were then evaluated using 2016-type coin cell. Cyclic voltammetry (CV) profiles in Fig. 3a and b show the first five CV curves of the NaNbO_3 anode for the Li/ NaNbO_3 cell, which was measured between 0.005 and 3 V (vs. Li/Li^+) at a scan rate of 0.2 mV s^{-1} . Clearly, the current density was noticeably reduced after the first cycle in the low voltage range due to the capacity loss and then remained almost unchanged for the following cycles. This is a typical behavior of niobium-based anode materials due to irreversible electrochemical reaction and formation of solid electrolyte interface. The cathodic peaks at 1.32 and 0.75 V can be attributed to Li^+ intercalate into crystalline NaNbO_3 to form $\text{Li}_x\text{NaNb}_{5-x}\text{O}_3$, and these redox peaks correspond to the valence variations of

$\text{Nb}^{5+}/\text{Nb}^{4+}$ and $\text{Nb}^{4+}/\text{Nb}^{3+}$. Notably, as shown in Fig. 3c and its inset, the NaNbO_3 nanocubes electrode showed narrower potential hysteresis (0.017 V) and higher peak currents and area, representing higher Li storage ability [15, 27]. This could be attributed to improved electronic conductivity of NaNbO_3 nanocubes due to its unique morphology. Figure 3d and Figure S1a showed the discharge/charge voltage profiles of the Li/ NaNbO_3 nanocubes and nanowires cell at different current densities (50, 100, 200, 300, 400, 500, 600, 700, 800, 900 and 1000 mA g^{-1}) in the potential range of 0.005–3.0 V. The discharge profiles of all current densities were characterized by featureless plateaus of a typical dominated surface-controlled kinetics (*i.e.*, pseudocapacitive properties), which were in good agreement with the small redox peaks in the CV plots.

Next, NaNbO_3 nanocubes were evaluated by galvanostatic discharge/charge at various current rates. As shown in Fig. 3e and Figure S1b, NaNbO_3 nanocubes exhibited excellent rate performance. The initial specific capacity of NaNbO_3 nanocubes was $\sim 161.8 \text{ mAh g}^{-1}$ at a current density of 100 mA g^{-1} . When the current density was changed to 1000 mA g^{-1} , a specific capacity of $\sim 124.7 \text{ mAh g}^{-1}$ was retained and finally recovered to $\sim 178.7 \text{ mAh g}^{-1}$ at a current density of 100 mA g^{-1} . In contrast, NaNbO_3 nanowires showed obviously lower specific capacity at each rate stages that only 104.3 mAh g^{-1}

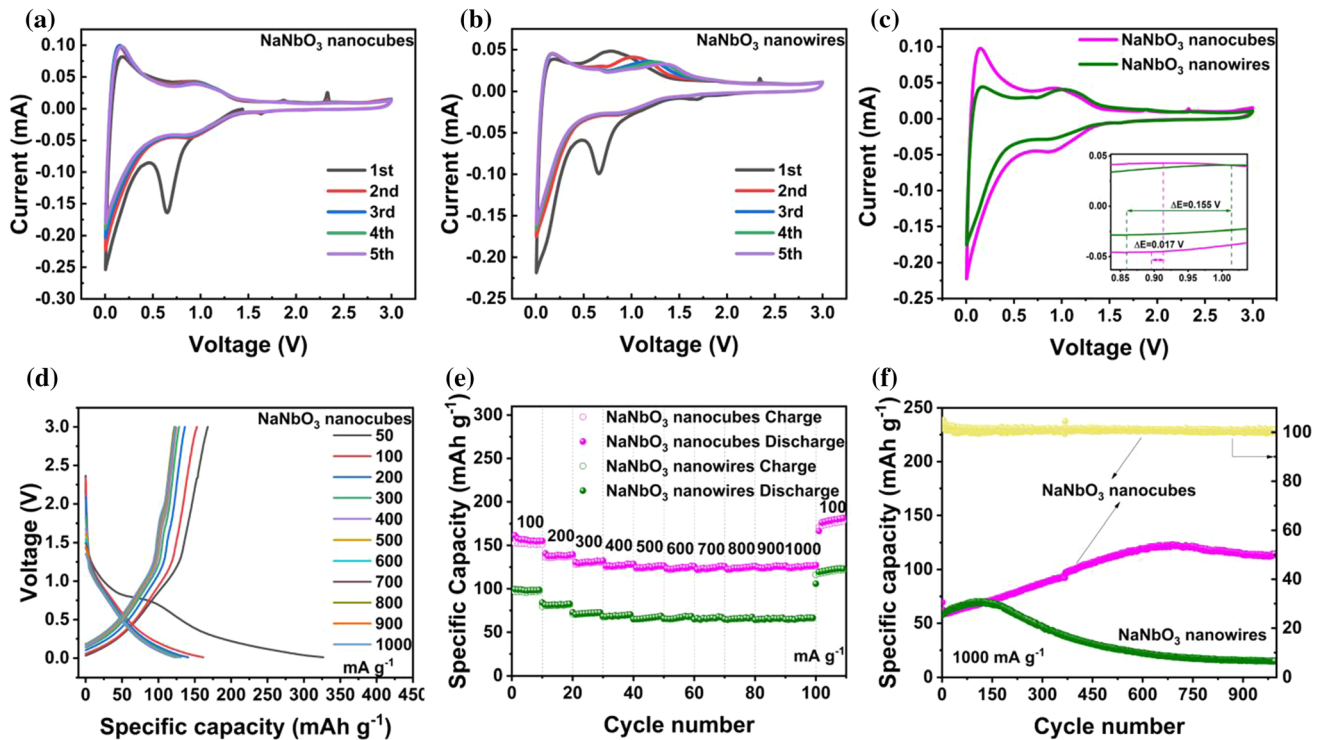


Figure 3 a,b Cyclic voltammograms for the first 5 cycles at a scan rate of 0.2 mV s^{-1} , c comparison of cyclic voltammograms, d initial charge/discharge curves, e rate performances of NaNbO_3

nanocubes and NaNbO_3 nanowires. f The long-term cycling performance of NaNbO_3 nanocubes and NaNbO_3 nanowires tested at a high current density of 1000 mA g^{-1} .

at a current density of 100 mA g^{-1} and 64.8 mAh g^{-1} at a current density of 1000 mA g^{-1} , indicating the cube morphology advantage of Li storage during charge/discharge.

In addition, good capacity retention over long cycles is crucial for the practical implementation of an electrode material. Therefore, long-term cycling performances of the NaNbO_3 nanocubes and nanowires were investigated. As shown in Fig. 3f, NaNbO_3 nanocubes displayed a higher reversible capacity retention than NaNbO_3 nanowires. At a current density of 1000 mA g^{-1} , an initial specific capacity of 69.5 mAh g^{-1} was achieved. After 1000 cycles, the capacity increased above 114.8 mAh g^{-1} , corresponding to a capacity retention of 165%. The excellent long-term cycling stability and the 100% coulombic efficiency indicated the high electrochemical stability and reversibility of NaNbO_3 nanocubes. The characteristic of gradually increased specific capacity of the NaNbO_3 nanocubes may be due to the persistent activation process during cycling indicating a new anode candidate bearing superior kinetics and stability for Li-ion storage.

In order to quantitatively analyze the pseudo-capacitance behavior in NaNbO_3 nanocubes and NaNbO_3 nanowires, the CV experiments were further implemented at a scan rate of 0.2 to 1 mV s^{-1} (Figs. 4a and d). The electrodes used for comparison were selected with the same quality of active material. Similar peak shapes could be observed during the anode and cathode processes, in which the redox peak current increased with the increasing scan rate. Obviously, the peak current of the NaNbO_3 nanocubes at each scan rate was greater than that of the NaNbO_3 nanowires, indicating that the NaNbO_3 nanocubes had the electrochemical activity of Li storage. The pseudocapacitive contributions behavior can be calculated according to Eq. (1) [40]:

$$I(V) = av + bv^{0.5} \quad (1)$$

where I and v refer to the current response at a given potential and scanning speed, a and b are adjustable parameters, and av and $bv^{0.5}$ represent the pseudo-capacitance contribution and the diffusion control contribution, respectively. At $0.2, 0.4, 0.6, 0.8$ and 1.0 mV s^{-1} , the pseudo-capacitance contributions of NaNbO_3 nanocubes could be reached to 57.3,

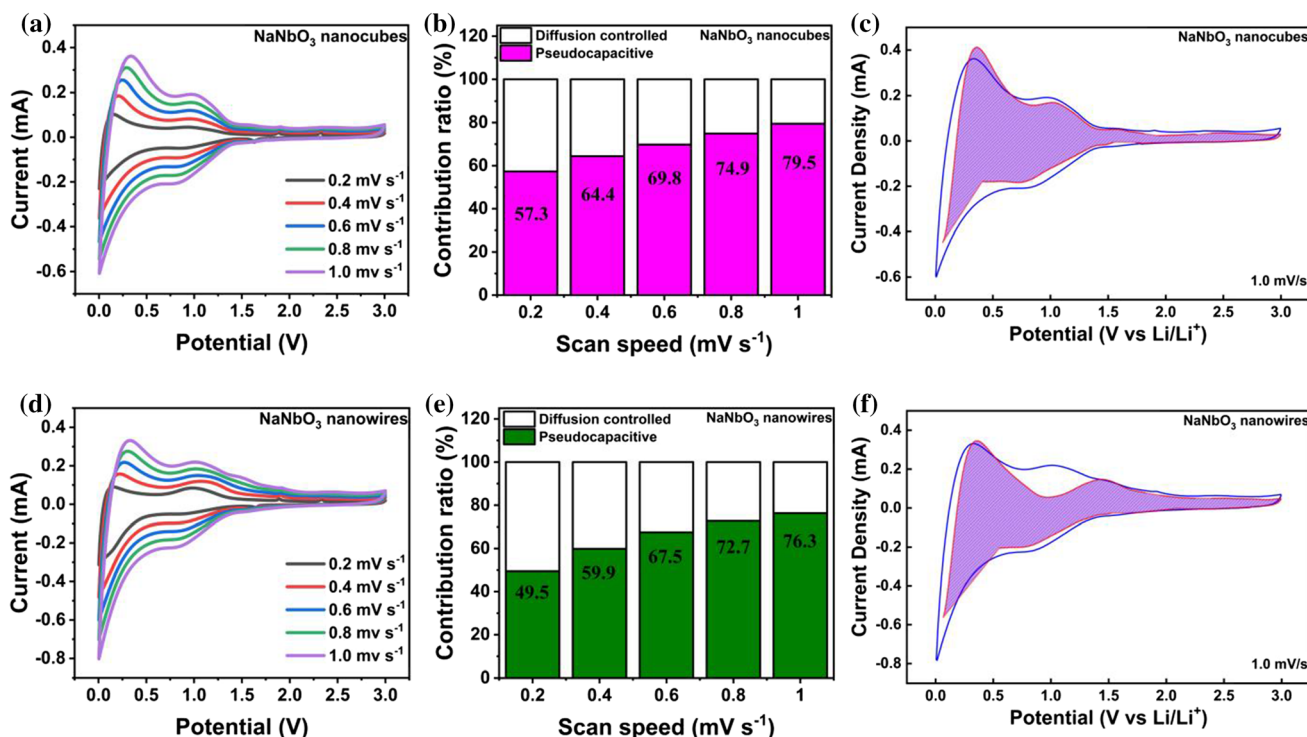


Figure 4 a, d The cyclic voltammograms of NaNbO₃ nanocubes and NaNbO₃ nanowires recorded at different scan rates. Percentages of pseudocapacitive contributions at different sweep

64.4, 69.8, 74.9 and 79.5%, respectively (Fig. 4b), demonstrating its significant pseudo-capacitance behavior between the slow and fast electrochemical reactions. Meanwhile, by contrast with NaNbO₃ nanocubes, the corresponding percentages of NaNbO₃ nanowires were decreased to 49.5, 59.9, 67.5, 72.7 and 76.3%, respectively (Fig. 4e). For a better understanding, the detailed pseudo-capacitance contribution in the potential range of 0.2 to 1.0 mV s⁻¹ was shown in the CV curve of 1.0 mV s⁻¹ (Fig. 4c, f and Figure S2). Therefore, it is confirmed that the NaNbO₃ nanocubes exhibited a more significant pseudo-capacitance effect at all scanning speeds.

The diffusion behaviors of lithium ions in NaNbO₃ nanocubes and NaNbO₃ nanowires were obtained through the CVs collected at different scanning rates of 0.2 ~ 1 mV s⁻¹. The linear relationship between the redox peak current (*I*_p) and the square root of the scan rate (*V*^{0.5}) is shown in Fig. 5a and b [41]. By deriving the classic Randles–Sevcik equation (Eq. (2)), the apparent Li diffusion coefficient *D* of NaNbO₃ nanocubes and NaNbO₃ nanowires for lithiation and delithiation can be calculated [42, 43]:

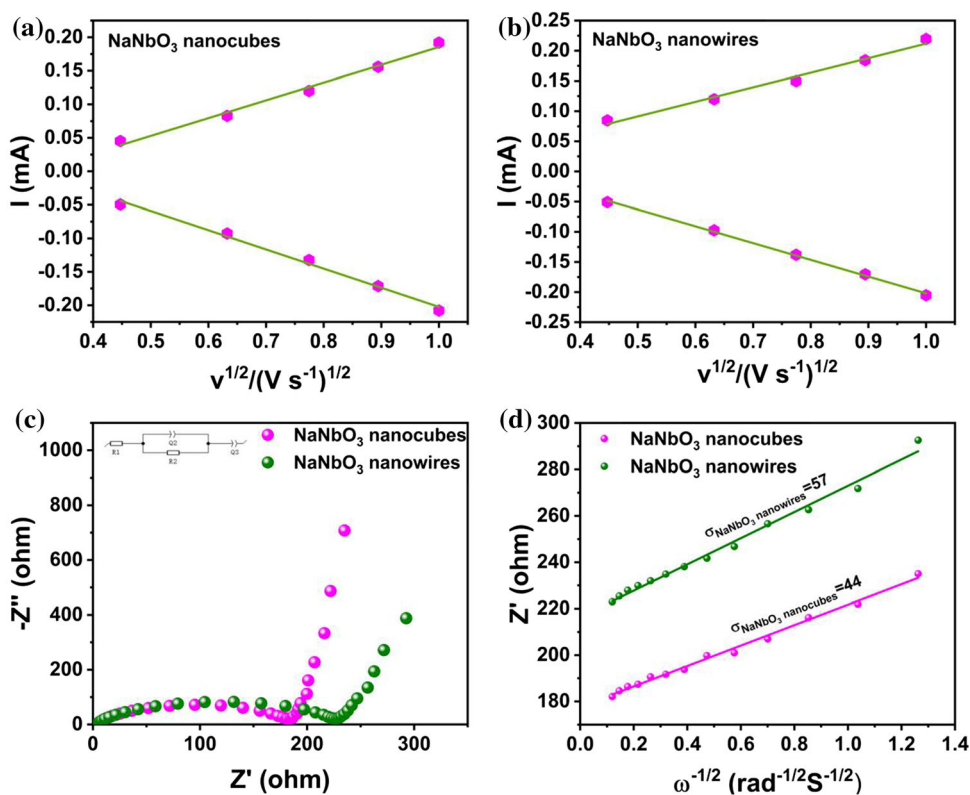
rates, and CV curves with detailed pseudocapacitive contributions at 1.0 mV s⁻¹ for b, e NaNbO₃ nanocubes and c, f NaNbO₃ nanowires.

$$I_p = 2.69 \times 10^5 \times n^{1.5} CSD^{0.5} V^{0.5} \quad (2)$$

where *n*, *C* and *S* are the number of charge transfers (Eq. (2)), the molar concentration of Li⁺ in the electrolyte (0.001 mol cm⁻³), and the geometric area of the electrode (1.54 cm²). It could be found that the *D*_{Li+} values of NaNbO₃ nanocubes were 4.78 × 10⁻¹³ cm² s⁻¹ for anode process and 4.09 × 10⁻¹³ cm² s⁻¹ for cathode process. For comparison, the *D*_{Li+} values of NaNbO₃ nanowires were 4.03 × 10⁻¹³ cm² s⁻¹ for anode process and 3.38 × 10⁻¹³ cm² s⁻¹ for cathode process. Apparently, the *D*_{Li+} value of NaNbO₃ nanocubes was greatly larger than NaNbO₃ nanowires, which could be explained by the larger unit volume of NaNbO₃ nanocubes (confirmed by the results of XRD) [37–39].

The potential electrochemical impedance spectroscopy (PEIS) diagram of NaNbO₃ nanocubes and NaNbO₃ nanowires is shown in Fig. 5c. Each plot consists of two recessed semicircles and a slope [44]. According to previous studies, the semicircle observed in the high-frequency region refers to the desolubilization, electron transfer and adsorption of Li⁺ ions, which is represented as R2/Q2 pairs in the

Figure 5 a, b The linear relationship between peak current and square root of the scan rate of NaNbO₃ nanocubes and NaNbO₃ nanowires. c Impedance spectrum and the equivalent circuit of NaNbO₃ nanocubes and NaNbO₃ nanowires. d The linear relationships between Z' and $\omega^{-1/2}$.



equivalent circuit (Fig. 5c inset). The slope observed in the low-frequency region corresponds to the Warburg resistance (Q3), which represents the diffusion of Li⁺ ions in the lattice of NaNbO₃ nanocubes and NaNbO₃ nanowires. R1 in the equivalent circuit reflects the ohmic resistance of the battery, which is mainly due to the electrolyte. The fitting R2 values of the NaNbO₃ nanocubes and NaNbO₃ nanowires were 180.7 and 223.3 Ω, respectively. Therefore, the NaNbO₃ nanocubes showed faster Li⁺ ion desolubilization, electron transfer, adsorption and Li⁺ ion insertion on the surface of active particles than NaNbO₃ nanowires, indicating its better electrochemical kinetics.

In addition, based on the EIS results, the Warburg factor and apparent Li⁺ ion diffusion coefficient of NaNbO₃ nanocubes and NaNbO₃ nanowires can be calculated using Eq. (3) [45]:

$$D = R^2 T^2 / 2 A^2 n^4 F^4 C^2 \sigma^2 \quad (3)$$

where D refers to the Li⁺ ion diffusion coefficient, R is the gas constant, T is the absolute temperature, C is the molar concentration of Li in the electrolyte, F is the Faraday constant, and S is the geometric area of the electrode, and σ embodies the Warburg factor

that can be obtained through Fig. 5d and Eq. (4) [46–48]:

$$Z' = R_0 + R_{ct} + \sigma \omega^{-0.5} \quad (4)$$

where Z' and ω represent the real impedance and the angular frequency, respectively. The calculated Li⁺ ion diffusion coefficients of NaNbO₃ nanocubes and NaNbO₃ nanowires were $4.88 \times 10^{-13} \text{ cm}^2 \text{ s}^{-1}$ and $2.91 \times 10^{-13} \text{ cm}^2 \text{ s}^{-1}$, respectively. It further proved that NaNbO₃ nanocubes have the ability to quickly migrate lithium ions, which was beneficial to the maintenance of charge and discharge under high current density.

Based on the aforementioned discussions, the optimal rate capability of NaNbO₃ nanocubes could be ascribed to several factors: (i) the better thermodynamic stability of NaNbO₃ nanocubes facilitated Li⁺ transportation and higher cycling stability; (ii) the superior electrochemical kinetics of NaNbO₃ nanocubes was beneficial for electron transfer, adsorption and Li⁺ insertion on the surface of active sites; (iii) NaNbO₃ nanocubes exhibited larger Li⁺ ion diffusion coefficient and significant pseudo-capacitance behavior. The combined effects of these three factors have significantly improved the rate capability.

Conclusions

In summary, NaNbO_3 nanocubes and NaNbO_3 nanowires were made by a simple hydrothermal reaction and were used as anode materials for $\text{M-Nb}^{\text{V}}\text{-O}$ embedded with Li-ion batteries. Comparative studies were explored to figure out the influence of morphology on the performance of Li-ion batteries. Experimental proves that NaNbO_3 nanocubes and NaNbO_3 nanowires have shared angle of NbO_6 octahedron forms a three-dimensional framework crystal structure, which leads to their large Li^+ ion diffusion coefficient. The unpaired 4d electrons in the Nb^{4+} ion led to its conductor characteristics and high conductivity. In particular, a significant pseudo-capacitance contribution is achieved in both slow and fast electrochemical reactions. Therefore, NaNbO_3 nanocubes and NaNbO_3 nanowires show excellent electrochemical performance. At 100 mA g^{-1} , NaNbO_3 nanocubes and NaNbO_3 nanowires can provide a high reversible capacity of $161.8/104.3 \text{ mAh g}^{-1}$. At 1000 mA g^{-1} , NaNbO_3 nanocubes and NaNbO_3 nanowires can still provide a high capacity of $124.7/64.8 \text{ mAh g}^{-1}$. Obviously, NaNbO_3 nanocubes exhibit better electrochemical performance than NaNbO_3 nanowires, which can be attributed to the better Li-ion diffusion abilities and higher pseudo-capacitance of NaNbO_3 nanocubes. Hence, this work provided a guide for the design of practical anode materials in the research community of high-performance Li-ion batteries.

Acknowledgements

We acknowledge the financial supports from National Natural Science Foundation of China (22002102, 21773291, 61904118), Natural Science Foundation of Jiangsu (BK20190935, BK20190947), Natural Science Foundation of the Jiangsu Higher Education Institutions of China (19KJA210005), Inner Mongolia Autonomous Region Key Laboratory of Nanocarbon Materials (No. MDK2019008), Post-graduate Research & Practice Innovation Program of Jiangsu Province (KYCX20_2588), Jiangsu Key Laboratory for Environment Functional Materials.

Declarations

Conflict of interest The authors declare no conflict of interests.

Supplementary Information: The online version contains supplementary material available at <http://doi.org/10.1007/s10853-022-07048-4>.

References

- Armand M, Tarascon JM (2008) Building better batteries. *Nature* 451(7179):652–657
- Goodenough JB, Kim Y (2010) Challenges for rechargeable Li batteries. *Chem Mater* 22(3):587–603
- Dunn B, Kamath H, Tarascon JM (2011) Electrical energy storage for the grid: a battery of choices. *Science* 334:928–935
- Zhang SS (2006) The effect of the charging protocol on the cycle life of a Li-ion battery. *J Power Sour* 161(2):1385–1391
- Arico AS, Bruce P, Scrosati B, Tarascon JM, Van Schalkwijk W (2005) Nanostructured materials for advanced energy conversion and storage devices. *Nat Mater* 4(5):366–377
- Song MY, Kim NR, Yoon HJ, Cho SY, Jin HJ, Yun YS (2017) Long-lasting Nb_2O_5 -based nanocomposite materials for Li-ion storage. *ACS Appl Mater Inter* 9(3):2267–2274
- Yan L, Chen G, Sarker S, Richins S, Wang H, Xu W, Rui X, Luo H (2016) Ultrafine Nb_2O_5 nanocrystal coating on reduced graphene oxide as anode material for high performance sodium ion battery. *ACS Appl Mater Inter* 8(34):22213–22219
- Liu G, Jin B, Bao K, Xie H, Guo J, Ji X, Zhang R, Jiang Q (2017) Facile synthesis of porous Nb_2O_5 microspheres as anodes for lithium-ion batteries. *Int J Hydrogen Energ* 42(9):6065–6071
- Wei M, Wei K, Ichihara M, Zhou H (2008) Nb_2O_5 nanobelts: a lithium intercalation host with large capacity and high rate capability. *Electrochem Commun* 10:980–983
- Wei M, Wei K, Ichihara M, Zhou H (2008) Nb_2O_5 nanobelts: a lithium intercalation host with large capacity and high rate capability. *Electrochem Commun* 10(7):980–983
- Kodama R, Terada Y, Nakai I, Komaba S, Kumagai N (2006) Electrochemical and in situ XAFS-XRD investigation of Nb_2O_5 for rechargeable lithium batteries. *J Electrochem Soc* 153(3):A583–A588

- [12] Liu Q, Zhang Q, Liu B, Dai WL (2020) Facile one-step hydrothermal synthesis of single-crystalline SnNb_2O_6 nanosheets with greatly extended visible-light response for enhanced photocatalytic performance and mechanism insight. *Nanotechnology* 32(6):065705
- [13] Liu Q, Zhang Q, Zhang L, Dai WL (2020) Highly efficient single-crystalline $\text{NaNb}_{1-x}\text{Ta}_x\text{O}_3$ ($x=0.125$) wires: the synergistic effect of tantalum-doping and morphology on photocatalytic hydrogen evolution. *J Mater Sci Technol* 54:20–30
- [14] Takashima T, Tojo T, Inada R, Sakurai Y (2015) Characterization of mixed titanium-niobium oxide $\text{Ti}_2\text{Nb}_{10}\text{O}_{29}$ annealed in vacuum as anode material for lithium-ion battery. *J Power Sour* 276:113–119
- [15] Tang K, Mu X, van Aken PA, Yu Y, Maier J (2013) Nano-earl-tring TiNb_2O_7 as anodes for rechargeable lithium batteries. *Adv Energy Mater* 3(1):49–53
- [16] Liu X, Wang H, Zhang S, Liu G, Xie H, Ma J (2018) Design of well-defined porous $\text{Ti}_2\text{Nb}_{10}\text{O}_{29}/\text{C}$ microspheres assembled from nanoparticles as anode materials for high-rate lithium ion batteries. *Electrochim Acta* 292:759–768
- [17] Wang T, Shi S, Kong F, Yang G, Qian B, Yin F (2016) The role of stable interface in nano-sized FeNbO_4 as anode electrode for lithium-ion batteries. *Electrochim Acta* 203:206–212
- [18] Wang T, Ge T, Shi S, Wu M, Yang G (2018) Synthesis of wolframite FeNbO_4 nanorods as a novel anode material for improved lithium storage capability. *J Alloy Compd* 740:7–15
- [19] Kumari TSD, Gandhi RV, Rahul G, Kamalanathan G, Kumar TP, Jeyakumar D, Lakshminarasimhan N (2014) Electrochemical lithium insertion behavior of FeNbO_4 : structural relations and in situ conversion into FeNb_2O_6 during carbon coating. *Mater Chem Phys* 145(3):425–433
- [20] Lou X, Fu Q, Xu J, Liu X, Lin C, Han J, Luo Y, Chen Y, Fan X, Li J (2017) $\text{GaNb}_{11}\text{O}_{29}$ nanowebs as high-performance anode materials for lithium-ion batteries. *ACS Appl Nano Mater* 1(1):183–190
- [21] Wang Z, Zheng R, Li Y, Yu H, Zhang J, Zhang X, Bi W, Shui M, Shu J (2020) Synthesis and characterization of $\text{GaNb}_{11}\text{O}_{29}/\text{C}$ for high-performance lithium-ion battery. *Ceram Int* 46(5):5913–5919
- [22] Kong F, Jiao G, Wang J, Tao S, Han Z, Fang Y, Yang G, Zhang L, Qian B (2017) Co-precipitation synthesis and electrochemical properties of CrNbO_4 anode materials for lithium-ion batteries. *Mater Lett* 196:335–338
- [23] Li Y, Zheng R, Yu H, Cheng X, Liu T, Peng N, Zhang J, Shui M, Shu J (2019) Observation of $\text{ZrNb}_{14}\text{O}_{37}$ nanowires as a lithium container via in situ and ex situ techniques for high-performance lithium-ion batteries. *ACS Appl Mater Inter* 11(25):22429–22438
- [24] Yang C, Zhang Y, Lv F, Lin C, Liu Y, Wang K, Feng J, Wang X, Chen Y, Li J, Guo S (2017) Porous $\text{ZrNb}_{24}\text{O}_{62}$ nanowires with pseudocapacitive behavior achieve high-performance lithium-ion storage. *J Mater Chem A* 5(42):22297–22304
- [25] Yan L, Lan H, Yu H, Qian S, Cheng X, Long N, Zhang R, Shui M, Shu J (2017) Electrospun $\text{WNB}_{12}\text{O}_{33}$ nanowires: superior lithium storage capability and their working mechanism. *J Mater Chem A* 5(19):8972–8980
- [26] Yan L, Shu J, Li C, Cheng X, Zhu H, Yu H, Zhang C, Zheng Y, Xie Y, Guo Z (2019) $\text{W}_3\text{Nb}_{14}\text{O}_{44}$ nanowires: ultra-stable lithium storage anode materials for advanced rechargeable batteries. *Energy Storage Mater* 16:535–544
- [27] Zhu X, Fu Q, Tang L, Lin C, Xu J, Liang G, Li R, Luo L, Chen Y (2018) $\text{Mg}_2\text{Nb}_{34}\text{O}_{87}$ porous microspheres for use in high-energy safe fast-charging and stable lithium-ion batteries. *ACS Appl Mater Inter* 10(28):23711–23720
- [28] Cheng X, Qian S, Yu H, Zhu H, Xie Y, Zheng R, Liu T, Shui M, Shu J (2019) $\text{BaNb}_{3.6}\text{O}_{10}$ nanowires with superior electrochemical performance towards ultrafast and highly stable lithium storage. *Energy Storage Mater* 16:400–410
- [29] Yan T, Ding R, Ying D, Huang Y, Huang Y, Tan C, Sun X, Gao P, Liu E (2019) An intercalation pseudocapacitance-driven perovskite NaNbO_3 anode with superior kinetics and stability for advanced lithium-based dual-ion batteries. *J Mater Chem A* 7(40):22884–22888
- [30] Park S, Sung J, Chae S, Hong J, Lee T, Lee Y, Cha H, Kim SY, Cho J (2020) Scalable synthesis of hollow $\beta\text{-SiC}/\text{Si}$ anodes via selective thermal oxidation for lithium-ion batteries. *ACS Nano* 14(9):11548–11557
- [31] Li H, Ren Y, Yang P, Jian Z, Wang W, Xing Y, Zhang S (2019) Morphology and size controlled synthesis of the hierarchical structured $\text{Li}_{1.2}\text{Mn}_{0.54}\text{Ni}_{0.13}\text{Co}_{0.13}\text{O}_2$ cathode materials for lithium ion batteries. *Electrochim Acta* 297:406–416
- [32] Wang C, Higgins D, Wang F, Li D, Liu R, Xia G, Li N, Li Q, Xu H, Wu G (2014) Controlled synthesis of micro/nanostructured CuO anodes for lithium-ion batteries. *Nano Energy* 9:334–344
- [33] Augustyn V, Come J, Lowe MA, Kim JW, Taberna PL, Tolbert SH, Abruña HD, Simon P, Dunn B (2013) High-rate electrochemical energy storage through Li^+ intercalation pseudocapacitance. *Nat Mater* 12(6):518–522
- [34] Liu H, Liang G, Gao C, Bi S, Chen Q, Xie Y, Fan S, Cao L, Pang WK, Guo Z (2019) Insight into the improved cycling stability of sphere-nanorod-like micro-nanostructured high voltage spinel cathode for lithium-ion batteries. *Nano Energy* 66:104100

- [35] Zhang K, Li Y, Wang Y, Zhao J, Chen X, Dai Y, Yao Y (2020) Enhanced electrochemical properties of iron oxalate with more stable Li^+ ions diffusion channels by controlling polymorphic structure. *Chem Eng J* 384:123281
- [36] Guo Y, Zhang L, Wang J, Liang J, Xi L (2019) Facile method for adjustable preparation of nano- Fe_7S_8 supported by carbon as the anode for enhanced lithium/sodium storage properties in Li/Na-ion batteries. *Electrochim Acta* 322:134763
- [37] Li J, Yao W, Zhang F, Rao X, Zhang Q, Zhong S, Cheng H, Yan Z (2021) Porous SnO_2 microsphere and its carbon nanotube hybrids: Controllable preparation, structures and electrochemical performances as anode materials. *Electrochim Acta* 388:138582
- [38] Song K, Seo DH, Jo MR, Kim YI, Kang K, Kang YM (2014) Tailored oxygen framework of $\text{Li}_4\text{Ti}_5\text{O}_{12}$ nanorods for high-power Li ion battery. *J Phys Chem Lett* 5(8):1368–1373
- [39] Kang K, Ceder G (2006) Factors that affect Li mobility in layered lithium transition metal oxides. *Phys Rev B* 74(9):094105
- [40] Kang K, Meng YS, Breger J, Grey CP, Ceder G (2006) Electrodes with high power and high capacity for rechargeable lithium batteries. *Science* 311(5763):977–980
- [41] Lu X, Wu G, Xiong Q, Qin H, Ji Z, Pan H (2017) Laser in-situ synthesis of SnO_2/N -doped graphene nanocomposite with enhanced lithium storage properties based on both alloying and insertion reactions. *Appl Surf Sci* 422:645–653
- [42] Mao W, Liu K, Guo G, Liu G, Bao K, Guo J, Hu M, Wang W, Li B, Zhang K, Qian Y (2017) Preparation and electrochemical performance of $\text{Ti}_2\text{Nb}_{10}\text{O}_{29}/\text{Ag}$ composite as anode materials for lithium ion batteries. *Electrochim Acta* 253:396–402
- [43] Hu R, Chen D, Waller G, Ouyang Y, Chen Y, Zhao B, Rainwater B, Yang C, Zhu M, Liu M (2016) Dramatically enhanced reversibility of Li_2O in SnO_2 -based electrodes: the effect of nanostructure on high initial reversible capacity. *Energy Environ Sci* 9(2):595–603
- [44] Augustyn V, Simon P, Dunn B (2014) Pseudocapacitive oxide materials for high-rate electrochemical energy storage. *Energy Environ Sci* 7(5):1597–1614
- [45] Liu H, Hu R, Sun W, Zeng M, Liu J, Yang L, Zhu M (2013) $\text{Sn}@\text{SnO}_x/\text{C}$ nanocomposites prepared by oxygen plasma-assisted milling as cyclic durable anodes for lithium ion batteries. *J Power Sources* 242:14–121
- [46] Yi T, Xie Y, Wu Q, Liu H, Jiang L, Ye M, Zhu R (2012) High rate cycling performance of lanthanum-modified $\text{Li}_4\text{Ti}_5\text{O}_{12}$ anode materials for lithium-ion batteries. *J Power Sources* 214:220–226
- [47] Churikov AV, Ivanishchev AV, Ivanishcheva IA, Sycheva VO, Khasanova NR, Antipov EV (2010) Determination of lithium diffusion coefficient in LiFePO_4 electrode by galvanostatic and potentiostatic intermittent titration techniques. *Electrochim Acta* 55(8):2939–2950
- [48] Nakayama M, Ikuta H, Uchimoto Y, Wakihara M (2003) Study on the ac impedance spectroscopy for the Li insertion reaction of $\text{Li}_x\text{La}_{1/3}\text{NbO}_3$ at the electrode-electrolyte interface. *J Phys Chem B* 107(38):10603–10607
- [49] Cheng M, Xia J, Hu J, Liu Q, Wei T, Ling Y, Li W, Liu B (2021) Nitrogen and oxygen codoped carbon anode fabricated facilely from polyaniline coated cellulose nanocrystals for high-performance Li-ion batteries. *ACS Appl Energy Mater* 4(9):9902–9912

Publisher's Note Springer Nature remains neutral with regard to jurisdictional claims in published maps and institutional affiliations.